JOURNAL OF MATERIALS SCIENCE **38** (2003) 4869–4874

Defect-free sintering of two material powder injection molded components

Part I *Experimental investigations*

D. F. HEANEY, P. SURI, R. M. GERMAN*
Center for Innovative Sintered Products, 147 Research West, The Pennsylvania State University, University Park, PA 16802-6809, USA
E-mail: rmg4@psu.edu

Two material powder injection molding (PIM) is a recently developed method to manufacture functionally graded components. This paper describes an experimental technique to determine the suitability of two materials to be combined via PIM. This is accomplished by comparing the individual shrinkage versus temperature behavior of the candidate systems. The concepts are validated by two material PIM, sintering, and subsequent microstructural observation. Two materials are compatible for two material powder injection molding provided they form a metallurgical bond and the sintering response of one material mimics the other. An extensive difference in sintering shrinkage, especially during the initial stage of sintering, results in defects such as cracks and delamination. Success of these concepts is elucidated by two material PIM of tool steel and boron doped austenitic stainless steel.

1. Introduction

Functional grading of components requires the design and fabrication of two or more material systems whose combination endows unique properties, specific to the desired application. An example is the production of wear resistant tool steel with a low alloy steel or stainless steel, where the low alloy steel or stainless steel can impart toughness, corrosion resistance, and an economical advantage as compared to a component that is fabricated of 100% tool steel [1]. Particulate materials processing offers attractive manufacturing routes such as injection molding, isostatic pressing, and tape casting to produce functionally graded components with a control of the microstructure and mechanical properties.

The powder injection molding route has two variants—over-molding and co-injection molding. In the over-molding variant, a molding machine equipped with two injection units is used to inject two different polymer-powder mixtures into the desired shape, as shown in Fig. 1. The method involves molding one part in a cavity and then rotating the tooling to form another cavity and molding around the previously molded part. When ejected from the mold, the component is composed of two interlocked materials. The molded part is then thermally processed to remove the polymer and sintered to produce a single, integrated component.

In co-injection molding, a functionally graded structure is produced using the flow behavior of the materials, through the same runner system, to produce a structured component that has a core and skin of two different materials. This is a well-established technology for plastics and has been experimentally examined for two metal and ceramic powders [1–3]. Fig. 2 illustrates the cross-sectional differences between over-molding and co-injection molding.

The barriers for the production of functionally graded components from particulate materials are similar irrespective of the production method or materials systems. It is widely recognized that the two material systems must have similar thermal expansion, similar densification behavior, and exhibit good interfacial bonding characteristics [4–9]. Further, a difference in sintering behavior during the early stage of sintering leads to defect formation since the compact is the weakest during this stage [6–9].

Pest *et al*. [4, 5] were among the first to apply the knowledge derived from dilatometry to demonstrate that a composite of M4 tool steel and Fe-2Ni (all compositions are in wt% unless otherwise specified) can be over-molded and thermally processed. Matching of the densification behavior of the powders was realized by altering the particle characteristics and alloy chemistry. In this case, the M4 powder was milled to promote solid state sintering at low temperatures and boron was admixed with the Fe-2Ni to form a liquid phase during sintering temperature. In general, their technique proved a moderate success; however, small cracks at the interface could not be avoided. Formation of defects despite modification of the shrinkage behavior was not successfully addressed in their study.

*Author to whom all correspondence should be addressed.

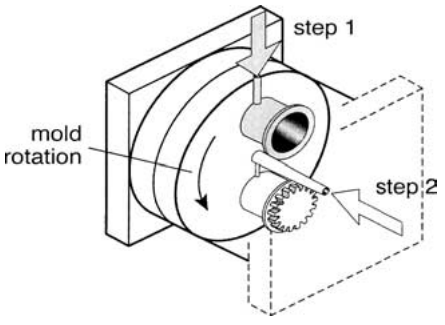

Figure 1 Schematic of the two material injection molding process. In the first step, the core material is molded, followed by mold rotation to mold the second material.

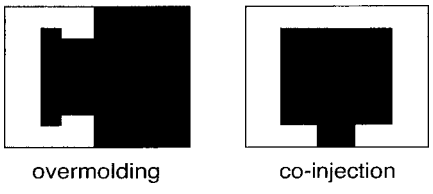

Figure 2 Schematic cross-section of an over molded and co-injection molded two material components.

Starting from tape-cast green sheets, Cai *et al.* [6] studied the co-sintering of alumina and zirconia. Sintering resulted in channel cracking defects in the layer under tension, delamination in the layer under compression, and debonding at the interface. These defects were attributed to a mismatch in both the sintering kinetics and thermal expansion. Modifications to the sintering profile and altering the particle chemistry by adding alumina to the zirconia eliminated the defects. However, neither the extent of mismatch stress nor sintering kinetics was successfully correlated to the formation or elimination of the defects during sintering.

In this paper, dilatometry is used as an experimental method to determine the compatibility of two metallic alloys for two material powder injection molding. Based on shrinkage behavior, two material systems exhibiting diverse characteristics are selected to identify and isolate the co-sintering behavior. A two material system was produced via injection molding by maintaining one material's densification characteristics (tool steel) and altering the sintering shrinkage characteristics of the other material by modifying its alloy chemistry. These results were subsequently used to develop a predictive model to determine the stress state during sintering and its effect on defect formation in Part II.

2. Experimental

The objective of this experimental study was to assess suitable material systems for co-sintering with tool steel without altering the metallurgical or functional characteristics of the tool steel powders. Furthermore, candidate systems were validated by two material powder injection molding. Multiple tool steel grades and multiple steel grades were examined for their shrinkage behavior during thermal processing. Dilatometry was used to select the systems with the most similar thermal shrinkage rate, thus most likely to give favorable interfacial integrity after injection molding and co-sintering.

The compositions of the different powders used in this study are given in Table I. The powder characteristics are detailed in Table II. The majority of the powders were gas atomized, except for the chromium powder and the carbonyl iron powder. Boron powder (amorphous, −325 mesh, 99.99% purity, Alfa Aesar) was admixed in the desired composition with the elemental or alloyed powders and homogenized by blending in a Turbula mixer (Glenn Mills Inc, Maywood, NJ) for 30 min.

3. Dilatometry study

The densification and expansion of the alloys were examined and compared to predict compatibility during

TABLE I Chemical composition of the powders

Powder	Fe	Cr	Co	Mo	V	W	Mn	Si	Ni	C	S	O	N
M2	Bal	3.9	–	4.7	1.8	6.1	0.29	0.37	–	0.961	0.017	0.049	0.005
D2	Bal	11.5	0.03	0.99	0.65	–	0.22	0.31	–	1.49	0.002	0.07	0.013
T15	Bal	4.2	4.8	0.32	4.6	12.0	0.19	0.21	–	1.53	0.11	0.06	–
4340	Bal	0.90	–	0.25	–	–	0.62	0.21	1.90	0.406	0.005	0.048	0.011
Fe	Bal	–	–	–	–	–	–	0.12	–	0.30	–	0.4	0.6
316L	Bal	17.1	–	2.2	–	–	1.4	0.49	10.6	0.03	0.008	0.038	0.186
Cr	0.1	99.6	<0.01	<0.01	<0.01	–	<0.01	<0.10	<0.01	–	–	–	–
Ni	0.1	–	<0.01	<0.01	–	<0.01	<0.10	99.8	–	–	–	–	

TABLE II Powder characteristics

Powder	T15	M2	D2	4340	316L	Fe	Cr	Ni
Vendor	UFP	UFP	UFP	UFP	UFP	ISP	F. W. winter	Inco
Theoretical density (g/cm^3)	8.00	8.05	8.00	7.86	7.9	7.78	7.23	8.96
Tap density (g/cm^3)	5.01	4.50	4.35	3.55	4.20	3.90	2.60	3.26
Apparent density (g/cm^3)	4.14	3.68	3.55	3.02	3.40	2.20	2.10	2.30
Particle size (μm)								
D_{10}	4.5	4.7	4.6	4.8	4.5	2.2	1.1	3.0
D_{50}	11.3	11.8	11.7	12.3	10.0	3.5	3.9	5.0
D_{90}	21.6	21.5	21.4	21.6	19.9	5.4	7.9	7.0

sintering using dilatometry. Powders were admixed with 2 wt% paraffin wax and pressed into 12.7 mm diameter and 10 mm long cylindrical compacts using a hand press (Carver Press, Wabash, IN) at a pressure of 100–150 MPa. The pressed cylindrical compacts were thermally debound at 575°C for 30 min in a flowing hydrogen atmosphere in a retort furnace. A vertical pushrod dilatometer (Anter, Pittsburgh, PA) was used to evaluate the dimensional changes of the presintered compacts during sintering at 10°C/min to 1400°C in an argon/hydrogen (95/5 vol%) atmosphere.

4. Two material powder injection molding

Based on the findings from the dilatometer study, boron (0.5 wt%) admixed 316L stainless steel and boron (0.5 wt%) admixed with Fe-10Cr steel made from elemental powders were each over-molded with M2 tool steel, as two contrasting systems. Powders were mixed with a 50 wt% wax - 50 wt% polyethylene binder system at a powder loading of 63 vol% for powder injection molding. A two-step injection molding process was employed to make a cylindrical green compact whose geometry is shown in Fig. 3. Initially, Material 1 was injection molded and followed by the overmolding of Material 2 in a 55 ton Arburg injection molding machine with a screw diameter of 25 mm. Samples were molded at an injection pressure of 500 bar, a volumetric rate of 30 cm^3/s, and an injection stroke of 25 cm. Melt and mold temperature were 170°C and 35°C, respectively.

The as-molded compacts were debound by a two-step process. First, a solvent debinding process was used to remove the wax from the compacts using 65°C heptane for 5 h. The compacts were air dried and thermally debound between 300 and 450°C and presintered at 850°C under flowing hydrogen gas in a retort furnace. Final sintering was performed at 1235°C in a 0.13 MPa (10^{-3} torr) vacuum for 30 min.

After processing, the compacts were evaluated for interfacial integrity using visual and microstructural evaluation. The selected compacts were mounted in Bakelite, ground with 320, 500 and 800 grit SiC paper and polished using 6 and 1 μm diamond paste for optical microscopy. Microhardness across the interface was determined using a Knoop indentor (Leco M-400-H, St. Joseph, MI) with 300 gram load.

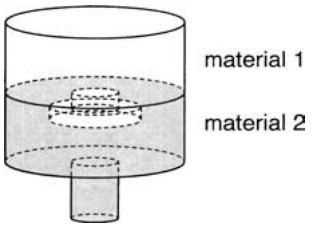

Figure 3 Cross-sectional geometry of the injection molded component used in this study.

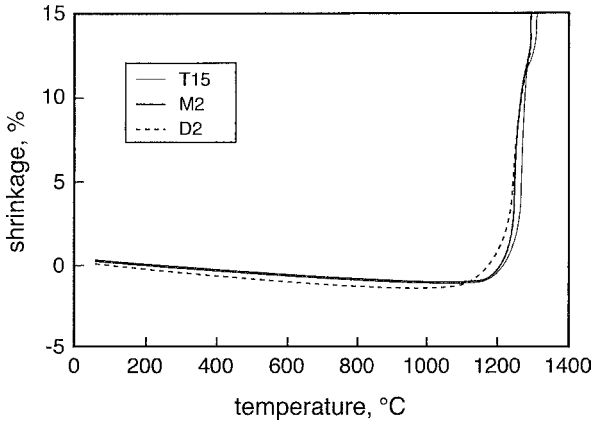

Figure 4 Dilatometer plot of sintering shrinkage versus temperature of tool steels sintered in argon-5% hydrogen atmosphere at a rate of 10°C/min to 1400°C for one hour. The density of the presintered compacts is approximately 60% of theoretical density.

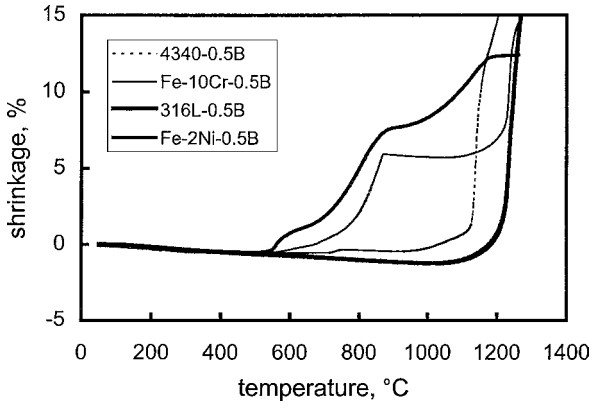

Figure 5 Dilatometer plot of sintering shrinkage versus temperature of candidate systems sintered in argon-5% hydrogen atmosphere at a rate of 10°C/min to 1400°C for one hour. The density of the presintered compacts is approximately 60% of theoretical density.

5. Results and discussion

The shrinkage behavior versus temperature, as determined by dilatometry, is given in Figs 4 and 5 for the tool steels and potential compatible materials, respectively. The relevant comparative dilatometry data is summarized in Table III. Fig. 4 indicates that all tool steel compositions have a similar sintering response with no observable shrinkage due to densification up to 1200°C and rapid shrinkage between 1200 and 1250°C. Further, Table III shows that the temperature at which maximum sintering shrinkage occurs for the D2 and M2 is within 6°C. Tool steels do not exhibit

TABLE III Dilatometry data for steel sample sintered in Ar/H_2

	Temperature at 0.1% shrinkage (°C)	Temperature at 0.1%/min shrinkage rate (°C)	Temperature at peak shrinkage rate (°C)
T15	1217	1192	1270
M2	1210	1195	1252
D2	1178	1159	1246
4340-0.5B	1044	1115	1145
316L-0.5B	1184	1177	1241
Fe-10Cr-0.5B	681	769	1239
Fe-2Ni-0.5B	618	557	829

any significant solid-state sintering and densification is due to supersolidus liquid phase sintering (SLPS) [10, 11]. The liquid phase forms due to the carbon content, present in the form of carbides. An increase in the carbon content increases the amount of liquid phase and decreases the sintering temperature of the tool steels [12, 13].

The potential compatible material's dilatometer data in Fig. 5 shows distinctly different sintering behaviors for these materials. A common feature in all these alloy systems is the formation of liquid phase due to the addition of boron. The 316L stainless steel admixed with boron exhibits very little solid-state sintering, similar to the tool steels. Densification is promoted via SLPS, with borides precipitating at the grain boundaries and forming a liquid phase with iron. The amount of boron influences the sintering window [14], the amount of liquid phase at the sintering temperature, the ensuing microstructure and mechanical properties [14–16]. The alloy 4340 admixed with boron shows little solid-state densification between 650 and 800°C. Rapid sintering shrinkage occurs between 1115 and 1170°C due to the formation of Fe-FeB_2 liquid phase leading to full densification. The rapid and full densification of the Fe-10Cr-0.5B alloy is observed at about the same temperature as the 316L-B alloy due to the formation of Fe-(Fe,Cr) boride liquid phase; however, it shows significant solid state sintering densification between 600°C and 825°C—contributed by the carbonyl iron powder [17]. With an increase in temperature, the $\alpha \rightarrow \gamma$ phase transformation retards further solid state sintering. Fe-2Ni-B also exhibits significant solid state sintering between 450 and 900°C. Subsequent shrinkage, leading to full densification is due to Fe-(Fe,Ni) boride liquid phase formation [18].

Figs 6 to 9 compare the difference in shrinkage behavior with temperature of M2 tool steel with 4340 Steel-0.5B, 316L-0.5B, Fe-10Cr-0.5B, and Fe-2Ni-0.5B compacts, respectively. It is evident from Fig. 6 that the sintering behavior of 4340 Steel-0.5B is very different than the M2 tool steel due to the greater than 15% difference in shrinkage during sintering. The 316L-0.5B stainless steel exhibits a sintering response very similar and compatible to that of M2 tool steel compositions up to 1200°C with a difference in shrinkage of less that 1%, as evident from Fig. 7. The Fe-10Cr-0.5B composition produced a fairly interesting result. Examination of Fig. 8 shows that the Fe-10Cr-0.5B composition has a distinctly different shrinkage behavior below 1200°C as compared to M2 tool steel; however, the shrinkage behavior of Fe-10Cr-0.5B is similar to M2 tool steel above 1200°C. Fig. 9 shows that there is a considerable difference in the sintering shrinkage behavior of Fe-2Ni-0.5B and M2, with Fe-2Ni-0.5B undergoing solid state densification and full densification via a liquid phase approximately 40°C before the onset of densification in tool steels. Based on these observations, the M2 tool steel was selected for

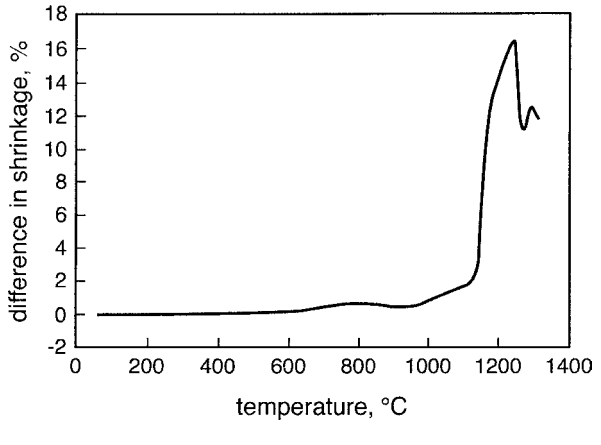

Figure 6 Difference in sintering shrinkage of 4340-0.5B steel with respect to M2 tool steel versus temperature.

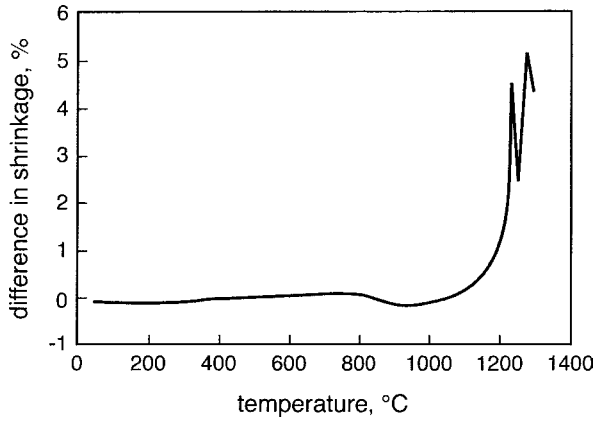

Figure 7 Difference in sintering shrinkage of 316L-0.5B stainless steel with respect to M2 tool steel versus temperature.

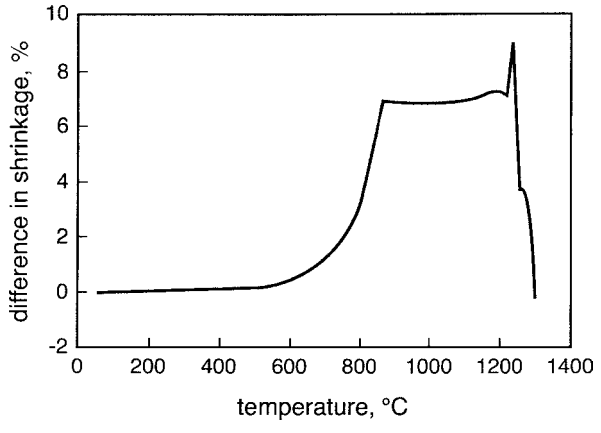

Figure 8 Difference in sintering shrinkage of Fe-10Cr-0.5B steel with respect to M2 tool steel versus temperature.

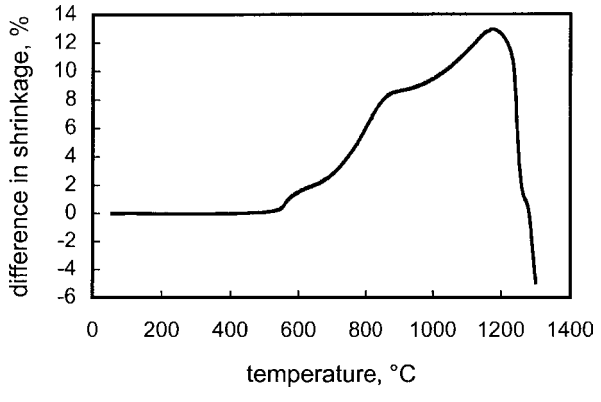

Figure 9 Difference in sintering shrinkage of Fe-2Ni-0.5B steel with respect to M2 tool steel versus temperature.

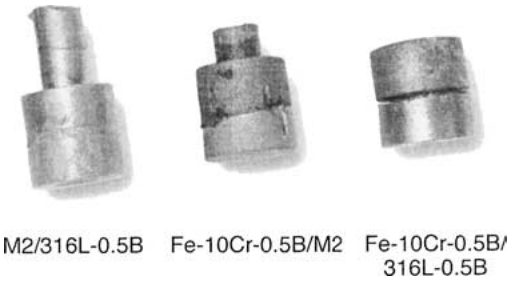

Figure 10 Picture showing the sintered two material PIM components. The M2/316L-0.5B combination sintered without defects while interface decohesion is evident in other material combinations.

two material powder injection molding with both the 316L-0.5B stainless steel and the Fe-10Cr-0.5B alloy.

Choice of atmosphere plays an important role during the sintering of tool steels and boron admixed steels. Tool steels can be sintered in a slightly reducing atmosphere containing nitrogen or in vacuum. The presence of nitrogen results in coarsening resistant MX type carbonitride precipitates leading to a refined microstructure [19]. Boron admixed steels on the other hand cannot be sintered in an atmosphere containing nitrogen as boron reacts with nitrogen to form BN, which reduces the amount of boron to form a liquid phase. Boron admixed steels can be sintered in hydrogen, a mixture of hydrogen and argon or vacuum. Based on the above constraints, the debound and presintered injection molded samples were sintered at 1235°C in 10^{-3} torr vacuum for 30 min.

The sintered samples produced at each condition are shown in Fig. 10. All compacts that contained Fe-10Cr-0.5B showed cracking at the interface between the two alloys after presintering at 850°C. As mentioned earlier, dilatometry data of the Fe-10Cr-0.5B alloy, as shown in Fig. 5, indicates that the compact undergoes significant solid-state sintering (up to 5% linear shrinkage) below temperature of 850°C. This solid state sintering is a characteristic of the carbonyl powder that was used as the ferrous component of the alloy. The large difference in shrinkage behavior induced cracks at the interface of the two alloys. This effect is particularly exaggerated for the co-sintered boron admixed 316L stainless steel and the Fe-10Cr-0.5B alloy. While the difference in sintering shrinkage above 1200°C is as high as 5%, the M2 tool steel and boron admixed 316L stainless steel system showed excellent results with no decohesion and a good diffusion bond. The difference in sintering shrinkage is observed at temperatures where the SLPS has initiated in the 316L-0.5B compact. Under such conditions, it is reasonable to assume that the compact is highly viscous and hence resistant to deformations as high as 5%.

The co-sintered 316L-0.5B and M2 tool steel sample was sectioned through the center along the length of the cylinder and polished to examine the microstructure. Fig. 11 shows the scanning electron micrographs of the interface of the co-sintered compact. The interface exhibited a good metallurgical bond. The M2 tool steel composition is identified by the blocky morphology of the precipitates (carbides) along the grain boundaries and distribution of the precipitates within the particles. The microstructure of the 316L-0.5B is identified by precipitation (of borides) along the grain boundaries. Hardness of the sample was measured on either sides of the interface. The reported value is an average of three measurements. The M2 had the highest hardness of 651 HK, 316L-0.5B stainless steel had a hardness of 257 HK, and the interface had hardness of 550 HK.

6. Conclusions

Sintering is a major barrier in producing a defect-free functionally graded component via PIM. Successful

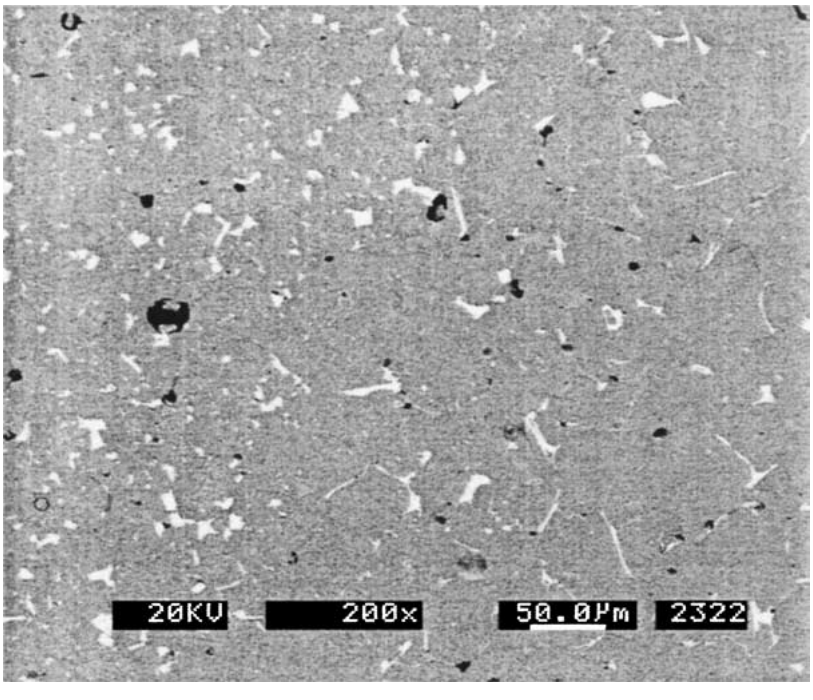

Figure 11 Scanning electron micrograph of M2 tool steel co-sintered at 1235°C with 316L-0.5B stainless steel. The M2 is on the upper left and the 316L-0.5B is on the lower right. The micrograph of the interface shows a good metallurgical bond at the interface.

sintering of two material PIM components require one material to mimic the densification behavior of the other material. In addition, the net shrinkage of the compacts after sintering should be equal. A prime choice for two material powder injection molding with the tool steels are austenitic stainless steels admixed with boron—both the materials have similar thermal expansion and sintering characteristics. Mismatch in the sintering behavior, especially in the initial stage of sintering increases the susceptibility to form defects. For example, Fe-10Cr-0.5B exhibits significant shrinkage compared to M2 during the initial solid state sintering resulting in cracking at the interface between the two materials. On the other hand, for the M2 and 316L-0.5B combination with a shrinkage mismatch of less than 0.2% during the initial stage sintering, difference in shrinkage as high as 5% after the initiation of liquid phase formation had no adverse effect on the integrity of the interfaces.

Acknowledgements

The authors wish to thank Lye King Tan and Advanced Materials Technologies Pte Ltd, Singapore, for supporting this research, and Patrick Sharbaugh, Graphic Designer at CISP for his assistance with figures and illustrations.

References

1. D. F. HEANEY, P. SURI and R. M. GERMAN, in Proceedings of the 2002 International Conference on Functionally Graded Materials—Technology Leveraged Applications, Denver, Colorado, edited by R. G. Ford and R. H. Hershberger (Metal Powder Industries Federation, Princeton, NJ, 2002) p. 105.
2. J. R. ALCOCK, M. W. DARLINGTON and D. J. STEPHENSON, *Powder Met.* **39** (1996) 252.
3. J. ALCOCK, *Metal Powder Report*, June (1999) 30.
4. A. PEST, F. PETZOLDT, T. HARTWIG, G. VELTL and H. EIFERT, in 1st European Symposium on PIM-1997, Munich, Germany, Oct. 15–16, 1997, p. 132.
5. A. PEST, F. PETZOLDT, T. HARTWIG and R. M. GERMAN, in Advances in Powder Metallurgy and Particulate Materials, edited by T. M. Cadle and K. S. Narasimham (Metal Powder Industries Federation, Princeton, NJ, 1996) Vol. 5, p. 19.
6. P. Z. CAI, D. J. GREEN and G. L. MESSING, *J. Amer. Ceram. Soc.* **80** (1997) 1929.
7. F. F. LANGE, *ibid.* **66** (1983) 396.
8. R. K. BORDIA and A. JAGOTA, *ibid.* **76** (1993) 2475.
9. F. F. LANGE, *Acta Metall.* **37** (1989) 397.
10. T. CHENG and R. RAJ, *J. Amer. Ceram. Soc.* **72** (1989) 1649.
11. R. M. GERMAN, *Intl. J. Powder Met.* **26** (1990) 23 and 35.
12. Z. Y. LIU, *Mater. Sci. and Eng.* A **293** (2000) 46.
13. C. S. WRIGHT, B. OGEL, F. LEMOISSON and Y. BIENVENU, *Powder Met.* **38** (1995) 221.
14. R. TANDON and R. M. GERMAN, *Intl. J. Powder Met.* **34** (1998) 40.
15. A. MOLINARI, J. KAZIOR, F. MARCHETTI, R. CANTERI, I. CRISTOFOLINI and A. TIZIANI, *Powder Met.* **37** (1994) 115.
16. H. I. BAKAN, D. F. HEANEY and R. M. GERMAN, *ibid.* **44** (2001) 235.
17. T. KOHNO, *Industr. Heat.*, February (1997) 57.
18. J. LIU, A. CARDAMONE, T. POTTER, R. M. GERMAN and F. J. SEMEL, *Powder Met.* **43** (2000) 57.
19. S. JAUGERI, F. FERNANDEZ, R. H. PALMA, V. MARTINEZ and J. J. URCOLA, *Met. Trans.* A **23A** (1992) 389.

Received 10 March
and accepted 14 August 2003